JACS
JOURNAL OF THE AMERICAN CHEMICAL SOCIETY

Article

pubs.acs.org/JACS

Hyperoxia Induces Intracellular Acidification in Neonatal Mouse Lung Fibroblasts: Real-Time Investigation Using Plasmonically Enhanced Raman Spectroscopy

Sajanlal R. Panikkanvalappil,[†] Masheika James,[‡] Steven M. Hira,[†] James Mobley,[§] Tamas Jilling,[‡] Namasivayam Ambalavanan,*[,‡] and Mostafa A. El-Sayed*[,†,∥]

[†]Laser Dynamics Laboratory, School of Chemistry and Biochemistry, Georgia Institute of Technology, Atlanta, Georgia 30332-0400, United States

[‡]Department of Pediatrics, University of Alabama at Birmingham, Birmingham, Alabama 35233, United States

[§]Department of Surgery, University of Alabama at Birmingham, Birmingham, Alabama 35233, United States

[∥]Department of Chemistry, King Abdulaziz University, Jeddah 21589, Saudi Arabia

Supporting Information

ABSTRACT: It is important to understand the molecular mechanisms underlying oxygen toxicity, which contributes to multiple human disorders. The archetype model of oxygen toxicity is neonatal lung injury induced by hyperoxia exposure. Here, we utilized plasmonically enhanced Raman spectroscopy (PERS) in combination with fluorescence and proteomic analysis to provide comprehensive information on hyperoxia-induced biomolecular modifications in neonatal mouse lung fibroblasts (nMLFs). During this study, we made the novel observation that hyperoxia induces intracellular acidification in nMLF, which we probed in real-time using label-free PERS. We found that intracellular acidification induces conformational modifications in proteins followed by significant changes in Raman vibrations corresponding to aromatic amino acids such as phenylalanine and tryptophan as well as cysteine moieties. Hyperoxia-induced intracellular pH changes and subsequent modifications in protein expression and associated post-translational modifications within the cells were further validated by fluorescence and proteomic analysis. These new insights may help identifying unique oxidant stress-induced mechanisms in disease processes and may guide the development of more efficient therapeutic strategies.

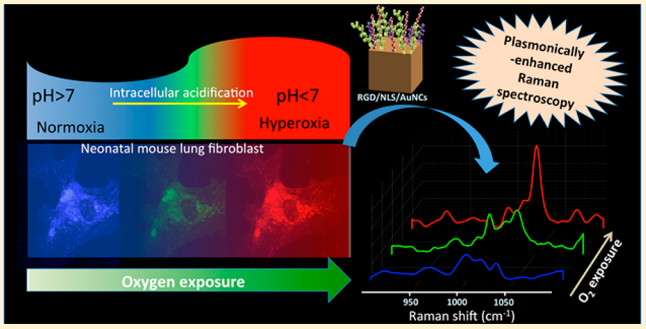

1. INTRODUCTION

Despite serving a vital role in sustaining life, oxygen in excess can also induce injury to developing lungs and other organs.[1,2] Supplemental oxygen is necessary to maintain sufficient tissue oxygenation in neonates with pulmonary disorders.[3−5] However, prolonged exposure to oxygen results in increased formation of reactive oxygen species (ROS) that may result in hyperoxia-induced acute lung damage associated with physiochemical modifications to biomolecules such as proteins, lipids, and nucleic acids.[2,6−9] Potential risks of hyperoxia in infants include bronchopulmonary dysplasia (BPD), abnormal immune responses, cardiopulmonary abnormalities, and other organ dysfunction.[8,10−12] In many cases, evidence suggests that direct oxidative damage through increased production of ROS is the key factor responsible for such damages.[2,13] However, the exact mechanisms of hyperoxia-induced cellular damage at the molecular level have not yet been adequately defined.[11]

It is important to prevent alveolar damage caused by hyperoxia in neonates requiring supplemental oxygen.[14] Hyperoxia-induced lung injury is not unique to neonates. Oxidant injury also contributes to lung diseases in adults such as idiopathic pulmonary fibrosis,[15,16] chronic obstructive pulmonary disease,[17] and lung cancer.[18] In this context, precise understanding of various physiochemical modifications within lung cells induced by hyperoxia, can enhance our knowledge of cellular responses and their long-term effects and thereby develop more efficient therapeutics. As hyperoxia and ROS-induced biomolecular events are highly dynamic in nature, simultaneous visualization of various physiochemical and conformational modifications to the biomolecules involved is challenging and requires high-throughput techniques.

Raman spectroscopy has shown promise in studying biomolecular events within living cells owing to its noninvasive nature and ability to differentiate spectral fingerprints of many molecules.[19−22] Plasmonically enhanced Raman spectroscopy (PERS), where the Raman signals can be enhanced by many folds of magnitude when the molecules probed are bound or in

Received: December 16, 2015
Published: March 3, 2016

DOI: 10.1021/jacs.5b13177
J. Am. Chem. Soc. 2016, 138, 3779−3788

very close vicinity to plasmonic field of the nanoparticles, further enhances the capabilities of this technique.[23−28] This can provide precise chemical information on biomolecular components inside the cells via sensitivity of vibrational bands to molecular conformation and environmental changes.[29,30] A variety of plasmonic nanoprobes (PNPs) are being used in PERS, which can be targeted to specific locations inside the cells and are capable of providing information on the biomolecules within the micro/nano environment of specific intracellular locations, in real-time.[31] In this study, we used PERS to probe in real-time the hyperoxia-induced cellular damages in neonatal mouse lung fibroblasts (nMLF). We made the novel observation that hyperoxia induces intracellular acidification in nMLF, which could be monitored in real-time using label-free PERS. Detailed proteomic analysis was performed in order to identify the hyperoxia-induced alterations in protein expression and post-translational modifications, which were in concordance with the PERS data. Our study illustrates the immense possibilities of PERS in real-time tracking of complex and dynamic biomolecular modifications in live cells and could provide new and vital information on hyperoxia-induced intracellular acidification and subsequent modifications in protein expressions and their damage as well as alteration of cell responses. This method has the potential to provide new insights on the role of intracellular acidification and associated biomolecular modification under hyperoxic conditions during the pathogenesis of many diseases.

2. EXPERIMENTAL SECTION

2.1. Materials. Hydrogen tetrachloroaurate trihydrate ($HAuCl_4 \cdot 3H_2O$), sodium borohydride ($NaBH_4$), ascorbic acid, cetyltrimethylammonium bromide (CTAB), phenylalanine, tryptophan, type 1 collagen, and trisodium citrate were purchased from Sigma-Aldrich USA. Custom-made peptides such as nuclear localization signal, NLS (CGGGPKKKRKVGG), and cell penetrating peptide, RGD (RGDRGDRGDRGDPGC), were procured from GenScript USA, Inc. Thiol-modified methoxypolyethylene glycol (mPEG-SH, MW 5000) was obtained from Laysan Bio, Inc.

2.2. Instrumentation. Transmission electron microscopic (TEM) images of gold nanocubes (AuNCs) were collected using a JEOL 100CX-2 microscope and their average size was determined using ImageJ software. A Renishaw inVia Raman Microscope coupled with Leica DM2500 M microscope was used to collect the DF images and PERS spectra from the nMLF cells. A 785 nm diode laser (Innovative Photonic Solutions) was used for the PERS measurements. The laser power was kept constant for all the experiments (∼6.2 mW).

2.3. Synthesis of Gold Nanocubes (∼37 nm Edge Length). AuNCs were synthesized as described earlier.[32] In a typical synthesis, seed nanoparticles were prepared by reducing a solution containing 2.75 mL $HAuCl_4 \cdot 3H_2O$ (0.909 mM) and CTAB (0.283 g in 5 mL deionized water (DI)) by an ice-cold 0.01 M $NaBH_4$ solution (600 μL) under stirring for 2 min. 0.35 mL of 10-fold diluted solution of this seed solution was allowed to grow in a growth solution for overnight. The growth solution was prepared by mixing CTAB solution (2.916 g in 400 mL DI water) with $HAuCl_4 \cdot 3H_2O$ (0.0394 g in 143 mL DI water) followed by the addition of 6 mL of ascorbic acid (1 M). The resultant AuNCs solution was purified by centrifugation at 9500*g* for 10 min followed by redispersion in DI water.

2.4. Preparation of PEG/RGD/NLS-Functionalized Gold Nanocubes (Plasmonic Nanoprobes (PNPs)). The purified AuNCs (10 mL of 1.56 nM) were first incubated with 123.22 μL of mPEG-SH (1 mM) for 24 h. This solution was purified by centrifugation at 9500*g* for 10 min. Afterward, these PEGylated AuNCs (9 mL of 1.62 nM) were treated with 4.14 μL of RGD (5 mM), and 10.65 μL of nuclear localization signal, NLS (5 mM), to yield PEG/RGD/NLS-functionalized AuNCs (PNPs). These PNPs were purified using centrifugation at 9500*g* for 10 min to remove unbound ligands and were redispersed in DI water for subsequent use. In order to avoid any influences due to the compositions of the three ligands on the PERS results, we made PNPs as described above in bulk quantity and used for all the experiments. Note that the surface functionality of the targeting nanoparticle plays a vital role in the PERS study.

2.5. Cell Culture. nMLF were isolated by explant culture from the periphery of lung from 1-day-old newborn mice as previously described.[33] nMLF cells were cultured in Dulbecco's modified Eagles' medium without L-glutamine (DMEM, Mediatech), which contains phenol red, supplemented with 10% v/v fetal bovine serum (FBS, Mediatech), 1% L-glutamine and 1% antibiotic-antimycotic solution (Mediatech) in a 37 °C CO_2 humidified incubator. For the PERS studies, the cells were grown on glass coverslips in complete growth medium in the incubator at 37 °C for 24 h. Subsequently, the cells were treated with 0.08 nM PEG/RGD/NLS-functionalized AuNCs, diluted in supplemented DMEM cell culture medium, for 24 h. The cells were then synchronized in the G_1 phase by serum starvation for 24 h. Afterward, the cells were released into complete medium and allowed to recover for ∼1−3 h before PERS experiments.

2.6. In Vitro PERS Measurements. PERS spectra were collected from the nMLF cells under various conditions in a time dependent manner. The spectra were measured from individual cells with a 1200 lines/mm grating using the Renishaw InVia Raman spectrometer. During the spectral acquisition, the laser was directed into a microscope and it was focused onto the sample by a 50×/0.75 N.A. objective. The backscattered signals from the samples (with an integration time of 10 s) were collected by a CCD detector in the range of 400 to 1800 cm^{-1}. A cubic spline interpolation was used for the baseline fit by manually selecting the points representative of the background. DF microscopy images were collected using Lumenera's infinity2 CCD digital camera.

2.7. Intracellular pH Measurements. Intracellular pH measurements were performed using carboxy-SNARF1 fluorescence pH indicator and live cell fluorescence digital imaging microscopy as described earlier.[34] Briefly, nMLF cells were grown on glass coverslips, washed in Krebs buffer (119 mM NaCl, 4.7 mM KCl, 1.2 mM KH_2PO_4 25 mM $NaHCO_3$, 2.5 mM $CaCl_2$, 1.2 mM $MgSO_4$), and then incubated with 5 μM of carboxy-SNARF1 acetoxymethyl ester, acetete (Life Technologies, Carlsbad, CA) in Krebs buffer at 37 °C in 5% CO_2, and ambient oxygen for 30 min. Cells on coverslips were washed again in Krebs, then transferred into a thermoregulated closed microscope-chamber (Bioptechs, Butler, PA) on a stage of a Nikon TE2000 inverted microscope equipped with epifluorescence illumination, a cooled CCD camera (Photometrics, Tucson, AZ) and Metafluor software (Molecular Devices, Sunnyvale, CA). Images at 485 nm excitation and 580 and 640 nm emission were captured at every 30 s while the chamber was perfused with Krebs buffer equilibrated with a gas mix of 21% oxygen, 74% nitrogen and 5% CO_2. In experiments when the effect of hyperoxia was evaluated the perfusate was switched to Krebs buffer equilibrated with 95% oxygen and 5% CO_2.

Fluorescence ratio to pH calibration was performed by switching from Krebs buffer to buffers containing depolarizing levels of K^+ (135 mM KCl, 2 mM K_2HPO_4, 20 mM HEPES, 1.2 mM $CaCl_2$, 0.8 mM $MgSO_4$) and pH adjusted to various pH levels between 6.8 and 8.0 and supplemented with 1 μM nigericin.

2.8. General Study Design/Proteomics Workflow. Cell pellets were acquired from nMLF (n = 3) following exposure to air (21% O_2, 5% CO_2, balance N_2) or hyperoxia (85% O_2, 5% CO_2, balance N_2) for 6 h, and the proteomic analysis was conducted. A total of 6 specimens were lysed in M-Per and the BCA protein quantification assay (Invitrogen) was performed to determine the protein concentration with minimal loss of sample. On the basis of the protein quant, an equal amount of each sample was used and first alkylated with IAA, then reduced and again alkylated with 4-vinyl-pyrimidine to map the dithiol linkages. They were then loaded and separated on a 4−12% Tris-Glycine and run either as a short stack (∼1 cm) or full way. Gels were stained with Colloidal Coomassie (Invitrogen) to both track the protein migration and as an additional QC for protein loading and

DOI: 10.1021/jacs.5b13177
J. Am. Chem. Soc. 2016, 138, 3779−3788

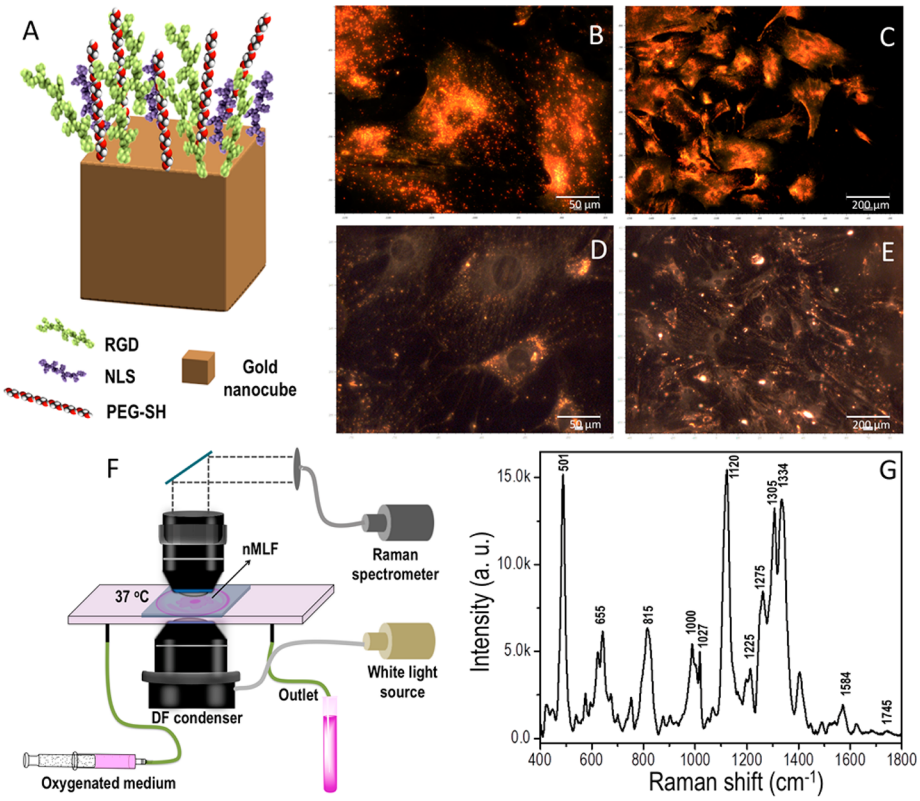

Figure 1. (A) Pictorial representation of the PNP used for the study. (B) and (C) are the DF images of nMLF cells, collected at different magnifications, after incubating with PNPs. The cells without PNPs are given in (D) and (E). (F) Pictorial representation of the experimental setup used for the real-time PERS monitoring of hyperoxia-induced cellular responses in nMLF cells. (G) PERS spectrum collected from nMLF cells. The spectra were collected from 12 different cells and spectra were averaged.

presentation. Each sample was cut into one gel piece for the short stack gels, and separately cut into 6-MW regions for each lane on the full runs. All gel pieces were processed and digested with trypsin in-gel overnight. The resultant peptides were then analyzed on by nano-LC–MS using a high resolution LTQ Orbitrap Velos Pro mass spectrometer (Thermo) as previously described.[35]

The LC–MS data were converted to a universal MzXML file format prior to being searched using SEQEST (Thermo) against a Mouse subset of the UniRef_100 database. These data were then uploaded to Scaffold (Proteome Software) in order to filter and group each peptide ID to specific proteins with peptide probability scores set at 80%, and protein probability scores set at 99%. Using only proteins presenting with 2 or more peptides per protein, the confidence interval was set @ ~99.9% with and FDR < 0.1. Quantification was carried out using Scaffold Q + using normalized spectral counts.

Statistical analysis was carried out initially on the entire set with stratification specific to proteins containing measurable signal in 2 of 3 specimens for both groups. Semi- and nonparametric tests were then applied each with a > 95% C.I., along with a fold change cutoff of ±1.5. The most significantly changed proteins were then further analyzed using Systems/Pathway analysis with MetaCore (Genego).

To highlight the most significant proteins, a "High Stats" analysis filter was applied, statistical analysis was separately carried out on the entire set with stratification specific to proteins containing measurable signal in 3 of 3 specimens for both groups. Semi- and nonparametric tests were then applied each with a > 95% C.I., along with a fold change cutoff of ±2.0. The most significantly changed proteins were then graphed and illustrated as bar charts.

3. RESULTS AND DISCUSSION

3.1. Obtaining Characteristic PERS Spectra of nMLFs.

Cellular responses to hyperoxia in nMLF cells were monitored in real-time using label-free PERS and dark-field (DF) microscopy (Figure 1). Here, functionalized gold nanocubes (AuNCs) having average size (edge length) of 37 nm were used as plasmonic nanoprobe (PNP) as it can enhance the intensities of Raman vibrations to a larger extent.[29,36,37] TEM image and extinction spectrum of AuNCs are given in Supporting Information 1 (Figure S1). In order to make the PNP, AuNCs were functionalized with thiol containing poly(ethyelene glycol) (PEG-SH) molecules, as it significantly reduces the cytotoxicity of the AuNCs. Besides that, the AuNCs were further functionalized with RGD (peptide sequence, which target $\alpha\beta$ integrins on the nMLF cell membrane to assist the uptake of nanoparticles through receptor-mediated endocytosis) and nuclear localization signaling (NLS) peptides (for targeting the nanocubes toward the nuclear region of nMLF cells)[38] (Figure 1A). RGD and NLS conjugated nanoparticles are known for targeting the nuclear region of variety of cells.[29,38] DF images of nMLF cells, treated with 0.08 nM PNPs for 24 h, showed intracellular localization of PNPs mainly in the cytoplasm and nuclear membrane regions (Figure 1B and C). The DF images of native nMLF cells (before treatment with the PNPs) collected at different magnifications are also shown in Figure 1D and E. Even though gold nanospheres (AuNSs) are also a good candidate for PERS studies, we used AuNCs for this study, as the uptake of AuNCs by the nMLF cells was relatively higher than that of AuNSs. Poor endocytosis of nanoparticle may affect the spectral reproducibility, which is critical for this study, and we hence chose AuNCs. Dark-field images of nMLF cells treated with 0.05 nM of PEG/RGD/NLS-functionalized AuNCs and AuNSs for 24 h under serum starvation are shown in the Supporting

DOI: 10.1021/jacs.5b13177
J. Am. Chem. Soc. 2016, 138, 3779–3788

Information 2 (Figure S2). The experimental setup used for live cell PERS studies is shown in Figure 1F. In order to obtain the characteristic PERS spectrum of the PNPs-internalized nMLF cells in G_1 phase, 785 nm laser was focused to reach the PNPs aggregates present inside the cytoplasm of the cells and spectra were collected from 12 different cells and were averaged (Figure 1G). The cells were synchronized to the G_1 phase using serum starvation in order to avoid any cell phase dependent spectral modifications during the experiments.

Tentative assignments of the Raman bands are given in Table 1. The Raman bands appeared at ∼501 and ∼655 cm^{-1} are mainly attributed to the vibrations corresponds to the disulfide (S−S) and C−S bonds of the sulfur containing amino acids, respectively.[39] The amide III vibration bands of proteins, which are considered to be the conformational marker bands of various polypeptide backbones, appeared as multiple bands in between 1215 and 1300 cm^{-1}.[29,40] The two bands appeared at around 1000 and 1027 cm^{-1} are attributed to the aromatic ring breathing (RB) vibration corresponds phenylalanine (Phe) and the C−H in-plane bending mode of Phe (contribution from RB vibration of tryptophan (Trp)), respectively.[41,42] The vibrational bands found in-between 1100−1150 cm^{-1} of the spectral region are mainly composed of the C−N vibration of amino acids and contribution from C−C stretching vibrations of the long-chain hydrocarbon backbone of the lipid. CH_2 bending mode of proteins and lipids along with methylene deformation appeared around 1420−1460 cm^{-1}. The intense Raman band around 1305 cm^{-1} is mainly attributed to the methylene twist vibrations.

Table 1. Tentative Assignments of Raman Bands in the PERS Spectra Collected from the nMLF Cells at Different Experimental Conditions[a]

tentative assignment of bands in the PERS spectra		
wavenumber (cm^{-1})	component	tentative assignments of PERS bands
495−510	protein	−S−S−
620−660	protein	−C−S−
800−850	proteins and lipid	Tyrosine and cysteine in proteins and C_4N^+, O−C−C−N symmetric stretches in lipids
1000−1010	protein	RB vibration of Phe
1012−1030	protein	In-plane bending mode of Phe and RB vibrationof Trp
1100−1140	lipid and protein	C−N vibration of proteins and Gauche and all-trans conformations of lipids
1170−1190	protein	In-plane CH bend of Phe
1200−1210	protein	C_6H_5−C stretching vibrations of Phe and Tyr
1215−1250	protein	Amide III (ß-pleated sheet)
1265−1300	protein	Amide III (α-helix)
1300−1325	protein and lipid	$-CH_2$ twist
1440−1460	protein and lipid	CH_2 bending mode of proteins and lipids along with methylene deformation
1584	protein	Phe

[a]RB = Ring breathing; Tyr = Tyrosine; Phe = Phenylalanine; Trp = Tryptophan.

For studying the cellular response and biomolecular modifications within nMLF cells during hyperoxia, the intracellular Raman spectra of the cells were collected in real-time as a function of time while the cells were being exposed to the oxygenated culture media. nMLF cells which showed good AuNCs uptake were chosen for the study. The live-cell chamber containing the coverslip with nMLF cells was kept at 37 °C. Before passing the oxygenated medium into the live cell chamber, PERS spectra were collected from the nMLF cell in order to ensure the spectral reproducibility. Afterward, oxygenated medium (O_2 of ultra high purity was bubbled through the medium for varying time (15, 30, and120 min)) was passed through the chamber (Figure 1F) and the Raman spectra were collected at regular intervals from the same cell.

3.2. Probing Cellular Responses of nMLFs toward Hyperoxia in Real-Time Using PERS. Hyperoxia induces the formation of various reactive oxygen species (ROS) such as superoxides, hydroxyl radical, hydrogen peroxide, peroxynitrite etc. within the cells.[2,11,13] These highly reactive species can cause cellular and subcellular damage via various biochemical reaction pathways such as lipid peroxidation, enzyme inactivation, and protein and nucleic acid degradation.[2,13,43−45] These ROS can target amino acid residues such as methionine, cysteine, phenylalanine, histidine, tryptophan, and tyrosine, which are susceptible to oxidation.[46,47] Time dependent PERS spectra were collected from nMLF cells incubated with normoxic cell culture medium and hyperoxic medium (pre-exposed to ultra high pure oxygen for 120 min), and are shown in Figure 2A and B, respectively. Under normoxic condition PERS spectra collected from nMLF cells did not show any significant spectral modifications. However, PERS spectra collected from cells treated with culture media, which was pre-exposed to oxygen for 120 min, resulted in drastic spectral modifications as shown in Figure 2B. After 30 min of the exposure the broad band that appeared around 1000−1030 cm^{-1} split into two distinct bands and centered around 1000 and 1027 cm^{-1}. This was accompanied by the emergence of spectral features in between 1500 and 1600 cm^{-1}. The phenyl ring bond-stretching vibrations correspond to aromatic amino acids such as phenylalanine (∼1584 cm^{-1}) and tryptophan (∼1550 cm^{-1}) as well as the amide II (1540−1570 cm^{-1}) band present in the proteins shows characteristic Raman vibrations in this region. A marked increase in the intensity of vibration of Raman band at 1745 cm^{-1} was also found after 30 min of oxygen exposure. This band is usually weak in the standard spectra of cells at G_1 phase (Figure 2A). The Raman vibration at 1027 cm^{-1} steadily increased with oxygen exposure and became a narrow and prominent band in the entire spectrum after 60 min. Furthermore, we noted that the intensity of vibration corresponding to the disulfide bond (∼500 cm^{-1}) substantially reduced and the ratio between the S−S and C−S (I_{S-S}/I_{C-S}) vibrations drastically decreased after ∼60 min.

The amide III vibration bands of proteins, which are considered as the conformational marker bands, found at 1260−1290 cm^{-1} (attributed to the amide III-α-helix structure) and 1210−1235 cm^{-1} (amide III-β-pleated sheet conformation)[40,48] showed noticeable changes under hyperoxic conditions. Upon oxygen exposure, intensity of vibration corresponding to β-conformation dominated over α-helix band after 45 min (Figure 2B), which is likely due to the conformational modification/misfolding of the proteins (evidence are given in the proteomics analysis section). Amide III-β conformation appeared as broad band due to the possible contribution from C_6H_5−C stretching vibrations of phenylalanine and tyrosine, which usually appears at 1205−1210 cm^{-1} in the normal Raman spectra.[41,49]

In order to study the influence of increasing degrees of hyperoxia on cellular responses and PERS spectra, we conducted the similar experiments by incubating the nMLF

DOI: 10.1021/jacs.5b13177
J. Am. Chem. Soc. 2016, 138, 3779−3788

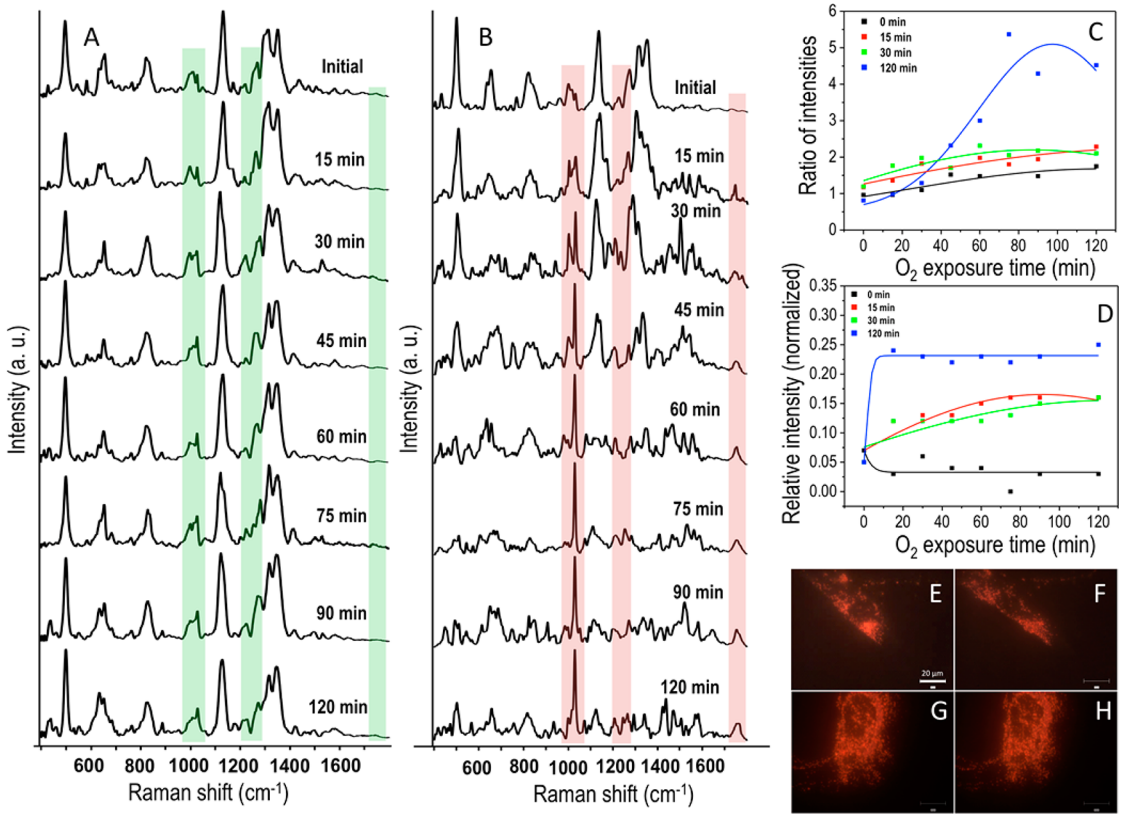

Figure 2. PERS spectra collected from the nMLF cells, which were incubated with normal medium (A) and oxygenated medium (pre-exposed to ultra high pure oxygen for 120 min) (B). Plots showing the ratio of intensities of I_{1027}/I_{1000} (C) and relative intensity of Raman vibration at 1745 cm^{-1} (D) collected as a function of time where the cells are incubated with the culture media, which are pre-exposed to oxygen for various time intervals (0, 15, 30, and 120 min). DF images of nMLF containing PNPs collected at 0 min (E) and 120 min (F) of oxygen exposure. DF images collected from the control experiments (without oxygen exposure) at 0 min (G) and 120 min (H). Scale bar shown in (E) is applicable to all DF images and is equal to 20 μm.

cells with hyperoxic cell culture media, for 15 and 30 min. PERS spectra collected at different time intervals from nMLF cells incubated with hyperoxic media for 15 and 30 min are given in Supporting Information 3 (Figure S3). Even though the spectral modifications were not as prominent as they were at 120 min exposure to hyperoxia, enhancement in the vibration at 1027 cm^{-1} and 1500−1600 cm^{-1} regions were obvious in both cases (15 and 30 min oxygen exposure). A decrease in the ratio between the S−S and C−S (I_{S-S}/I_{C-S}) vibrations was also noted in both cases upon prolonged oxygen exposure. The Raman band at 1745 cm^{-1} also emerged in these two cases, where the cells were incubated with 15 and 30 min oxygenated culture media. Additional PERS spectra collected (before and after hyperoxia treatment) from two randomly selected cells in different cases are given in the Supporting Information 4 (Figure S4). In all the cases, the spectra showed similar trend, which validates the observed hyperoxia-induced intracellular acidifications and biomolecular modifications.

Plots showing the ratio of intensities of I_{1027}/I_{1000} and relative intensity of Raman vibration at 1745 cm^{-1} collected as a function of time are shown in Figure 2C and D, respectively. Here, the cells were incubated with the culture media, which were pre-exposed to oxygen for various time intervals (0, 15, 30, and 120 min). A drastic enhancement in the I_{1027}/I_{1000} ratio was obvious at extreme hyperoxic conditions (120 min oxygen expsoure). The intensity of vibration at 1745 cm^{-1} was also higher under this condition than normal (0 min oxygen expsoure) and lower levels of hyperoxia (15 and 30 min oxygen expsoure). The nMLF cells did not show any significant morphological change after 120 min under normal conditions (Figure 2G and H). However, under hyperoxic conditions (120 min oxygen expsoure), the cells shrunk slightly (Figure 2E and F).

3.3. Discussion of the PERS Spectra and Origin of Raman Band at 1027 cm^{-1}. The broad Raman band appearing at 1725−1765 cm^{-1} is mainly attributed to the carbonyl stretching vibration in esters and carboxylic acid groups (COOH/COOR)[50] of biomolecules formed within the cytoplasm during hyperoxia. It is known that lipid peroxidation produces compounds containing carbonyl groups, which has a vibration in this region.[43,51] Earlier studies in flies suggest that hyperoxia can irreversibly enhance the carbonyl contents.[47] Apart from this, the characteristic C═O stretching band in protonated carboxyl group (COOH) usually appears in 1700−1750 cm^{-1} region.[52,53] This points out the possibility that the observed Raman spectral modifications under hyperoxia could be due to the hyperoxia-induced intracellular acidification in nMLF cells. It is known that acidic environment can catalyze the esterification reactions of many biomolecules especially fatty acids.[54]

In order to identify the contribution of intracellular acidic environment toward the Raman vibration found at 1745 cm^{-1}, a control experiment was performed, where PERS of cysteine was collected from its native and acidified form. Here, the nanoparticles were mixed with 10 mM of cysteine solution and were then incubated for 120 min. Afterward, the PERS

DOI: 10.1021/jacs.5b13177
J. Am. Chem. Soc. 2016, 138, 3779−3788

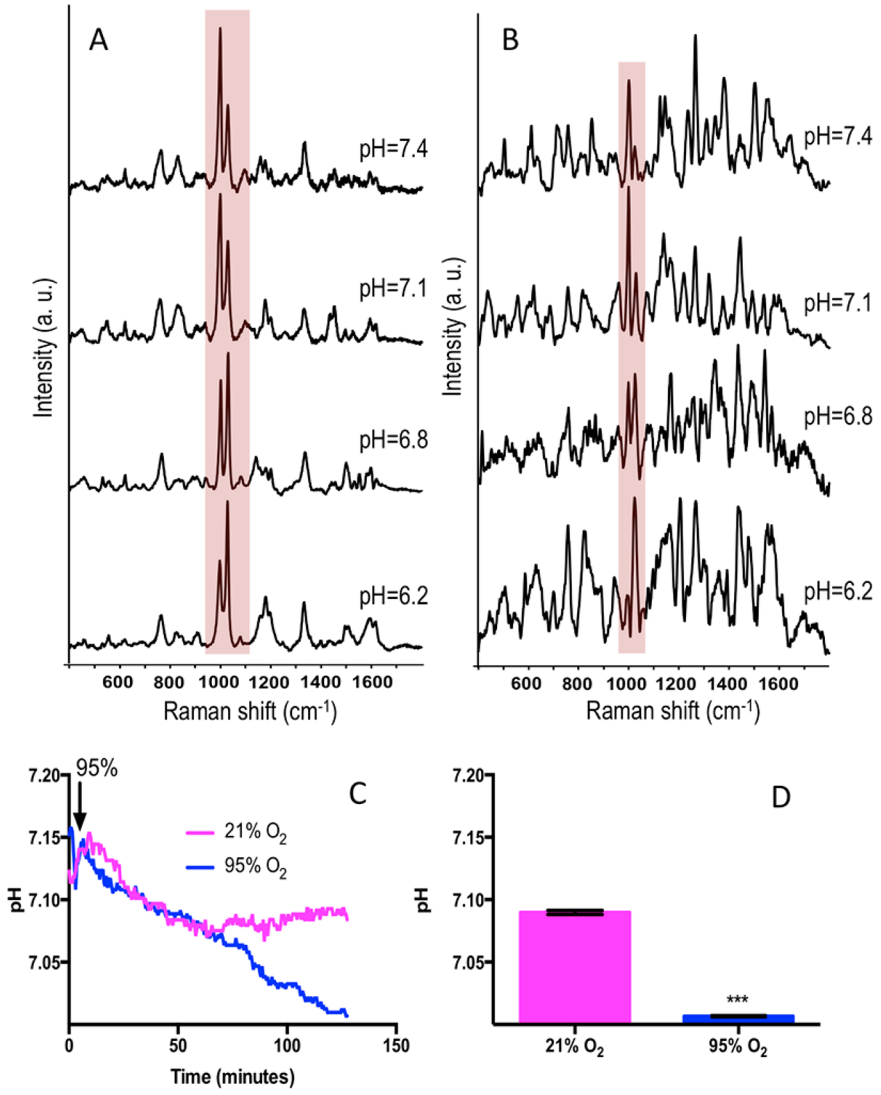

Figure 3. PERS spectra of phenylalanine (A) and type 1 collagen (B) collected at different pH. (C) and (D) are the plots and histograms, respectively, showing intracellular acidification in nMLF cells (measured by using the pH-sensitive fluorescent dye SNARF) under hyperoxia (blue line in plot C) compared to normoxic condition (red line in plot C).

spectrum was collected from the dried sample. PERS spectra of cysteine collected at native and acidic environment are given in Supporting Information 5 (Figure S5). Appearance of the Raman band at ~1738 cm^{-1} after protonation pointing toward the involvement of cysteine moiety in contributing to the broad Raman band observed at 1725−1765 cm^{-1} in the PERS spectra of nMLF cells under hyperoxic conditions. A shift from the intensity maximum may be due to a combination band corresponding to the carbonyl stretching vibration in esters and protonated carboxylate residue. A shift is also expected, as the intracellular cysteine residue is associated with peptide bond in a particular proteins and it is not associated with individual free cysteines (modifications in the spatial configurations of the proteins may also contribute). Hyperoxia is well-known to generate free radicals. Free radicals generated during hyperoxia may also induce lipid peroxidation and exposure of hydrophobic aromatic amino acid residues of lipoproteins/proteins. Significant reduction of the Raman vibration appeared at 1100−1150 cm^{-1} (Figure 2B), which is mainly attributed to the combination of the C−N vibration of amino acids and contribution from C−C stretching vibrations of the long-chain hydrocarbon backbone of the lipid also supports this argument.

In order to unravel the origin of the sharp band at 1027 cm^{-1} and to investigate the pH dependence of this band, we conducted another control experiment where the PERS spectra were collected from native and protonated phenylalanine. We chose this aromatic amino acid as it shows strong Raman vibrations in this region (1000−1030 cm^{-1}).[41] Interestingly, a strong enhancement in the vibration corresponding to the C−H in-plane bending mode of phenylalanine (1027 cm^{-1}) was observed upon protonation (Figure 3A). The PERS of phenylalanine collected at different pH using AuNCs, showed a gradual increase in the intensity of vibration at 1027 cm^{-1} (Figure 3A). These results confirm that the sharp band observed at 1027 cm^{-1} during the exposure of nMLF cells to hyperoxia is mainly due to the intracellular acidification and subsequent enhancement in the C−H in-plane bending vibration of phenylalanine (with contribution from tryptophan). These spectral features can only be originated from intracellular proteins, as the targeted AuNCs used throughout these studies do not contain phenylalanine or tryptophan. A

DOI: 10.1021/jacs.5b13177
J. Am. Chem. Soc. 2016, 138, 3779−3788

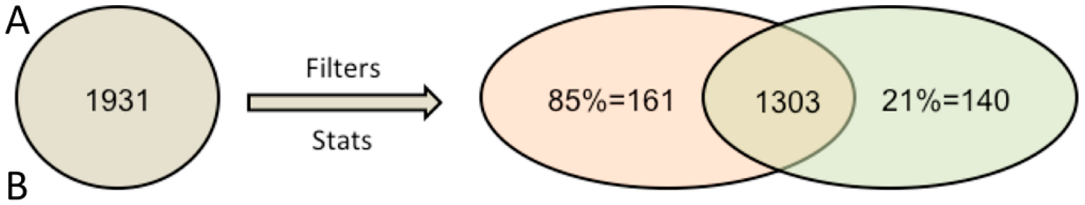

Protein Name	21_1	21_2	21_3	85_1	85_2	85_3	SAM	Ttest	Fold (85/21)
26S proteasome non-ATPase regulatory subunit 5	5.3	11.6	8.4	1.0	3.8	2.7	1.3	0.033	-3.4
Peptidyl-prolyl cis-trans isomerase FKBP9	5.3	6.3	4.2	2.0	1.9	0.9	2.2	0.006	-3.3
Ubiquitin-associated protein 2-like	7.4	7.4	6.3	1.0	0.9	4.6	1.8	0.023	-3.2
CD90.1	7.4	8.4	5.3	4.0	0.9	1.8	1.5	0.011	-3.1
Mitogen-activated protein kinase 3	6.3	5.3	5.3	2.0	1.9	2.7	3.2	0.001	-2.5
Serine/arginine-rich-splicing factor 2	4.2	4.2	5.3	1.0	0.9	3.7	1.2	0.040	-2.4
Fission 1 (Mitochondrial outer membrane) homolog (Yeast), isoform CRA_c	8.4	7.4	8.4	3.0	3.8	3.7	4.6	0.000	-2.3
Cyclin-dependent kinase 4	9.5	10.5	10.5	4.0	3.8	6.4	2.6	0.006	-2.2
Dual specificity mitogen-activated protein kinase kinase 1	5.3	8.4	8.4	3.0	2.8	4.6	1.4	0.023	-2.1
Very long-chain specific acyl-CoA dehydrogenase, mitochondrial	6.3	7.4	4.2	3.0	1.9	3.7	1.2	0.029	-2.1
N(G),N(G)-dimethylarginine dimethylaminohydrolase 2	16.8	17.9	10.5	11.1	5.6	5.5	1.1	0.031	-2.0
NADPH--cytochrome P450 reductase	6.3	5.3	2.1	7.1	12.2	8.2	0.9	0.043	2.0
Arylsulfatase B	1.1	2.1	1.1	3.0	1.9	3.7	1.0	0.046	2.0
Alpha-N-acetylglucosaminidase (Sanfilippo disease IIIB)	2.1	1.1	1.1	3.0	2.8	2.7	1.9	0.023	2.0
Heterogeneous nuclear ribonucleoproteins A2/B1	14.7	11.6	8.4	31.3	24.4	16.4	1.2	0.042	2.1
60S ribosomal protein L6	2.1	2.1	5.3	6.1	5.6	8.2	1.1	0.031	2.1
Ribosome binding protein 1	9.5	6.3	5.3	12.1	19.7	12.8	1.2	0.032	2.1
Neural cell adhesion molecule 1	2.1	1.1	1.1	2.0	3.8	3.7	1.1	0.035	2.2
Phosphoribosylformylglycinamidine synthase	3.2	3.2	5.3	7.1	9.4	10.0	1.8	0.007	2.3
Hexose-6-phosphate dehydrogenase (Glucose 1-dehydrogenase)	1.1	2.1	2.1	5.1	2.8	4.6	1.3	0.026	2.4
Src substrate cortactin	10.5	4.2	5.3	11.1	18.8	17.4	1.2	0.021	2.4
40S ribosomal protein S12	2.1	5.3	4.2	13.1	7.5	7.3	1.1	0.043	2.4
TAR DNA-binding protein 43	2.1	4.2	3.2	10.1	4.7	8.2	1.2	0.045	2.4
Glycine cleavage system H protein, mitochondrial	2.1	2.1	2.1	7.1	4.7	3.7	1.7	0.048	2.4
Actin-related protein 2/3 complex subunit 5	9.5	2.1	3.2	10.1	15.0	11.9	1.1	0.032	2.5
Procollagen-proline, 2-oxoglutarate 4-dioxygenase (Proline 4-hydroxylase), alph	3.2	2.1	5.3	7.1	12.2	7.3	1.2	0.032	2.5
Vesicular integral-membrane protein VIP36	5.3	5.3	2.1	11.1	14.1	8.2	1.5	0.017	2.6
Collagen alpha-2(I) chain	6.3	11.6	4.2	21.2	23.5	18.3	2.1	0.005	2.8
UDP-glucuronosyltransferase 1-7C	1.1	1.1	1.1	4.0	2.8	2.7	2.9	0.018	3.0
Major vault protein	4.2	4.2	1.1	9.1	11.3	9.1	2.2	0.004	3.1
Ras GTPase-activating protein-binding protein 1	1.1	2.1	1.1	3.0	6.6	5.5	1.5	0.031	3.6
Erythrocyte band 7 integral membrane protein	1.1	2.1	3.2	11.1	8.4	4.6	1.4	0.039	3.8

Figure 4. (A) Statistics showing 301 proteins significantly changed in their abundance (161↑ and 140↓ in 85% vs 21% O_2) during hyperoxia. (B) The top 32 protein abundances changed (High Stats) in 85% vs 21% O_2 treated nMLF cells.

comparative PERS spectra of protonated and nonprotonated phenylalanine and tryptophan along with nMLF cells exposed to 120 min oxygenated media for 75 min is given in Supporting Information 6 (Figure S6). This clearly shows the pH dependence on the Raman feature emerged at 1027 cm^{-1}. Protonation of tryptophan resulted in the broadening of the sharp band at 1016 cm^{-1} and the appearance of shoulder bands at 1027 cm^{-1}. Additionally, the PERS spectra of 0.1 mM of phenylalanine dissolved in normal and oxygenated water (prepared by continuously purging the ultrahigh pure oxygen into the deionized water for 60 min) were also analyzed (see Supporting Information 7, Figure S7). Absence of any noticeable difference in the spectral features rule out any oxygen-induced significant chemical and conformational modification to phenylalanine as well as any possible Raman enhancing effect on AuNCs due to the hyperoxic conditions. Further, the role of intracellular acidic pH on the enhancement of C−H in-plane bending mode of phenylalanine (also contribution from tryptophan) vibration observed at 1027 cm^{-1} was confirmed by collecting the PERS spectra of a protein. Here we used type 1 collagen as a model protein. The PERS spectra of collagen collected at various pH are given in Figure 3B. Acidification of collagen showed a distinct enhancement in the 1027 cm^{-1} vibration, which is obvious in the spectra.

In order to validate the PERS results, intracellular pH measurements were performed using carboxy-SNARF1 fluorescence pH indicator and live cell fluorescence digital imaging microscopy.[34] The cells exposed to normoxia showed a gradual drift toward acidic intracellular pH, which stabilized at pH 7.09. We attribute this drift to the transfer of cells from stagnant tissue culture medium into constant perfusion with normoxic oxygenated (relatively hyperoxic) perfusate. However, the cells exposed to hyperoxia at 95% O_2 exhibited continuing drift toward more acidic pH until the carboxy-SNARF-1 dye began leaking from the cells excessively when the cells reached pH 7.0. These results clearly validate the PERS data. Details on the experimental procedure of this study are given in the Experimental Section.

3.4. nMLF Response to Hyperoxia Treatment: Proteomic Analysis. To study the proteins involved in the hyperoxia response, proteomic analysis was conducted for the nMLF samples at normoxic (21% O_2) and hyperoxic (85% O_2) conditions. After filtering the data, 1931 proteins were identified with <0.1% FDR. Of those, 1303 proteins were found to be identified in >66% of specimens in both arms. We have found that at least 60% of samples per statistical arm must have quantifiable peptides for an n = 3−4 study in order to obtain robust analysis. From the proteomics analysis, we found that 301 were significantly changed in abundance (161↑ and 140↓ in 85% vs 21% O_2) (Figure 4A). In order to highlight the most significant proteins, we then focused on the High Stats proteins (mentioned in the Experimental Section), and found 32 differentially abundant hits (21↑ and 11↓ in 85% vs 21% O_2), which are illustrated in Figure 4B. Among these 32 proteins, which changed in abundance under hyperoxia, 21 proteins were found to be increased during hyperoxia and 11 proteins were decreased (Figure 5A and B).

A significant enhancement in the heterogeneous nuclear ribonucleoproteins A2/B1 as well as collagen alpha-2(1) chain

DOI: 10.1021/jacs.5b13177
J. Am. Chem. Soc. 2016, 138, 3779−3788

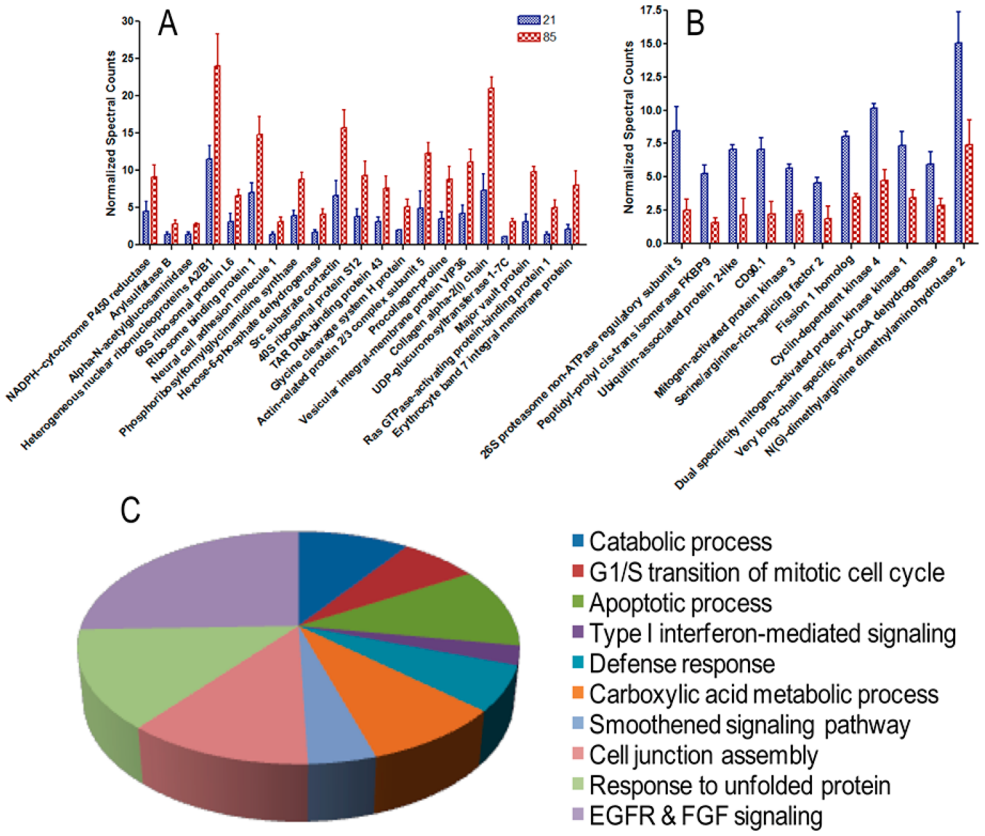

Figure 5. Most significant proteins increased (A) and decreased (B) in nMLF exposed to 85% vs 21% O_2. (C) Using Systems analysis, the most significant biological processes were identified from this study, and are highlighted in the pie chart as the percent of protein hits associated with each process.

was obvious when the nMLF cells exposed to 85% O_2 for 5 h. The observed modifications in the Raman vibrations under hyperoxia are most likely associated with the up-expression of these 21 proteins. We also noticed that collagen contains significant amount of phenylalanine and can change its conformation under acidic condition so as to give intense Raman vibration corresponding to the C−H in-plane bending mode of phenylalanine at around 1027 cm^{-1} (Figure 3B). Furthermore, we quantified oxidized proteins during hyperoxia and could identify oxidative modifications of disulfide linkage in certain proteins (Supporting Information 8; Figure S8A), which was in concordance with the PERS data. The proteomic results also suggest that hyperoxia can induce oxidation of tryptophan and produces various oxidized form of tryptophan such as hydroxykynurenine and kynurenine (Figure S8B). A similar modification corresponds to the tryptophan ring breathing vibration was also observed in the PERS spectra.

From the systems analysis, several biological processes were found to be more significant under hyperoxic conditions, which are given in the pie chart as the percent of protein hits associated with each process (Figure 5C). Among them, epidermal growth factor receptor (EGFR) and fibroblast growth factor (FGF) signaling were identified as most significant (80%). EGFR and FGFs play key role in regulating various cellular functions such as proliferation, differentiation, regulation of angiogenesis, and wound healing in adults.[55−57] Even though FGF signaling has tumor suppressive functions in certain contexts, unusual FGF/FGFR signaling pathway can promote many developmental disorders including cancer.[55] Significant alterations in the expressions of EGFR and FGF in the nMLF exposed under hyperoxic condition need special attention as it may play a critical role in aberrant lung development.

We also noticed that unfolded protein response (UPR) was significantly altered (34.9%) during hyperoxia, which is considered as a mechanism that senses unfolded or misfolded proteins and subsequent activation of the endoplasmic reticulum (ER) stress receptors.[58,59] It has been recognized that the ER stress plays a crucial role on the development of a wide range of human diseases, including pulmonary fibrosis, neurodegeneration, metabolic disorders, heart diseases, and cancer.[58,60] The PERS spectra also validate this result as there was an obvious protein conformational modification observed during hyperoxic condition (Figure 2). As a result of hyperoxia, apart from an enhancement in the vibration corresponds to the amide III-β conformation, the Raman vibrations corresponds to aromatic amino acids became more prominent in the PERS spectra. It is likely that the hyperoxia-induced intracellular modifications and pH modifications could probably perturb the conformation or induce misfolding of the proteins in the nano/microenvironment of the PNPs so as to expose the hydrophobic amino acid residues to the plasmonic field of the PNPs, which are generally found buried within proteins.[61,62]

4. CONCLUSION

We explored the unique possibilities of plasmonically enhanced Raman spectroscopy together with fluorescence and proteomics analysis to evaluate hyperoxia-induced cellular events in nMLF in real-time. Hyperoxia induced significant modifications in the Raman spectral features of nMLF cells, which can be

DOI: 10.1021/jacs.5b13177
J. Am. Chem. Soc. 2016, 138, 3779−3788

mainly attributed to the lowering of intracellular pH and associated changes in protein expression and conformational modifications. Raman data suggest that the extent of damage to the intracellular biomolecules is directly related to the duration of oxygen exposure. The role of acidic environment in the observed Raman spectral modifications was further confirmed by various control experiments. Using proteomic analysis, we identified several proteins up and down regulated during hyperoxia, which need special attention as it may play a critical role in aberrant lung development and may promote many developmental disorders including cancer. These findings provide further evidence that, apart from the reactive oxygen species-mediated cellular damage during hyperoxia, lowering of intracellular pH may also play important role in causing cellular toxicity in nMLF cells.

■ ASSOCIATED CONTENT

Supporting Information

The Supporting Information is available free of charge on the ACS Publications website at DOI: 10.1021/jacs.5b13177.

TEM images and UV−vis extinction spectra of AuNCs, comparison of DF images of nMLFs targeted with AuNCs and AuNSs, additional PERS spectra of cells under different hyperoxic conditions, PERS spectra of amino acids under various conditions, proteomics data showing oxidative modification in proteins. (PDF)

■ AUTHOR INFORMATION

Corresponding Authors

*nambalavanan@peds.uab.edu

*melsayed@gatech.edu

Notes

The authors declare no competing financial interest.

■ ACKNOWLEDGMENTS

The authors at the Georgia Institute of Technology wish to thank NSF-DMR grant (1206637) for support. NA acknowledges support from NIH-U01 HL122626; NIH-R01 HD066982; NIH-R01 HL129907. JM wishes to acknowledge support from NIH-NCI (P30CA13148-38).

■ REFERENCES

(1) Hetz, S. K.; Bradley, T. J. *Nature* **2005**, *433*, 516.

(2) Auten, R. L.; Davis, J. M. *Pediatr. Res.* **2009**, *66*, 121.

(3) Bookatz, G. B.; Mayer, C. A.; Wilson, C. G.; Vento, M.; Gelfand, S. L.; Haxhiu, M. A.; Martin, R. J. *Pediatr. Res.* **2007**, *61*, 698.

(4) Lodha, A.; Sauvé, R.; Bhandari, V.; Tang, S.; Christianson, H.; Bhandari, A.; Amin, H.; Singhal, N. *PLoS One* **2014**, *9*, e90843.

(5) Carlo, W. A.; Finer, N. N.; Walsh, M. C.; Rich, W.; Gantz, M. G.; Laptook, A. R.; Yoder, B. A.; Faix, R. G.; Das, A.; Poole, W. K.; Schibler, K.; Newman, N. S.; Ambalavanan, N.; Frantz, I. D.; Piazza, A. J.; Sánchez, P. J.; Morris, B. H.; Laroia, N.; Phelps, D. L.; Poindexter, B. B.; Cotten, C. M.; Van Meurs, K. P.; Duara, S.; Narendran, V.; Sood, B. G.; O'Shea, T. M.; Bell, E. F.; Ehrenkranz, R. A.; Watterberg, K. L.; Higgins, R. D. *N. Engl. J. Med.* **2010**, *362*, 1959.

(6) Jamieson, D.; Chance, B.; Cadenas, E.; Boveris, A. *Annu. Rev. Physiol.* **1986**, *48*, 703.

(7) Deuber, C.; Terhaar, M. *J. Perinat. Neonatal Nurs.* **2011**, *25*, 268.

(8) Tateda, K.; Deng, J. C.; Moore, T. A.; Newstead, M. W.; Paine, R.; Kobayashi, N.; Yamaguchi, K.; Standiford, T. J. *J. Immunol.* **2003**, *170*, 4209.

(9) Dasgupta, C.; Sakurai, R.; Wang, Y.; Guo, P.; Ambalavanan, N.; Torday, J. S.; Rehan, V. K. *Am. J. Physiol. Lung Cell Mol. Physiol.* **2009**, *296*, L1031.

(10) Baleeiro, C. E. O.; Wilcoxen, S. E.; Morris, S. B.; Standiford, T. J.; Paine, R. *J. Immunol.* **2003**, *171*, 955.

(11) Bhandari, V.; Choo-Wing, R.; Lee, C. G.; Zhu, Z.; Nedrelow, J. H.; Chupp, G. L.; Zhang, X.; Matthay, M. A.; Ware, L. B.; Homer, R. J.; Lee, P. J.; Geick, A.; de Fougerolles, A. R.; Elias, J. A. *Nat. Med.* **2006**, *12*, 1286.

(12) Ramani, M.; Bradley, W. E.; Dell'Italia, L. J.; Ambalavanan, N. *Am. J. Respir. Cell Mol. Biol.* **2014**, *52*, 594.

(13) Brueckl, C.; Kaestle, S.; Kerem, A.; Habazettl, H.; Krombach, F.; Kuppe, H.; Kuebler, W. M. *Am. J. Respir. Cell Mol. Biol.* **2006**, *34*, 453.

(14) Mach, W. J.; Thimmesch, A. R.; Pierce, J. T.; Pierce, J. D. *Nurs. Res. Pract.* **2011**, *2011*, 1.

(15) Walters, D. M.; Cho, H. Y.; Kleeberger, S. R. *Antioxid. Redox Signaling* **2008**, *10*, 321.

(16) Kinnula, V. L.; Myllarniemi, M. *Antioxid. Redox Signaling* **2008**, *10*, 727.

(17) Taraseviciene-Stewart, L.; Voelkel, N. F. *J. Clin. Invest.* **2008**, *118*, 394.

(18) Valavanidis, A.; Vlachogianni, T.; Fiotakis, K.; Loridas, S. *Int. J. Environ. Res. Public Health* **2013**, *10*, 3886.

(19) Puppels, G. J.; de Mul, F. F. M.; Otto, C.; Greve, J.; Robert-Nicoud, M.; Arndt-Jovin, D. J.; Jovin, T. M. *Nature* **1990**, *347*, 301.

(20) Harada, I.; Takeuchi, H. Raman and ultraviolet resonance Raman spectra of proteins and related compounds. In *Spectroscopy of Biological Systems, Advances in Spectroscopy*; Clark, R. J. H.; Hester, R. E., Eds.; John Wiley & Sons: Chichester, U.K., 1986; p 113.

(21) Barman, I.; Dingari, N. C.; Saha, A.; McGee, S.; Galindo, L. H.; Liu, W.; Plecha, D.; Klein, N.; Dasari, R. R.; Fitzmaurice, M. *Cancer Res.* **2013**, *73*, 3206.

(22) Zavaleta, C. L.; Garai, E.; Liu, J. T. C.; Sensarn, S.; Mandella, M. J.; Van de Sompel, D.; Friedland, S.; Van Dam, J.; Contag, C. H.; Gambhir, S. S. *Proc. Natl. Acad. Sci. U. S. A.* **2013**, *110*, E2288.

(23) Panikkanvalappil, S. R.; Mahmoud, M. A.; Mackey, M. A.; El-Sayed, M. A. *ACS Nano* **2013**, *7*, 7524.

(24) Panikkanvalappil, S. R.; Mackey, M. A.; El-Sayed, M. A. *J. Am. Chem. Soc.* **2013**, *135*, 4815.

(25) Li, M.; Kang, J. W.; Sukumar, S.; Dasari, R. R.; Barman, I. *Chem. Sci.* **2015**, *6*, 3906.

(26) Aikens, C. M.; Madison, L. R.; Schatz, G. C. *Nat. Photonics* **2013**, *7*, 508.

(27) Chaudhari, K.; Pradeep, T. *J. Biomed. Opt.* **2015**, *20*, 046011.

(28) Madiyar, F. R.; Bhana, S.; Swisher, L. Z.; Culbertson, C. T.; Huang, X. H.; Li, J. *Nanoscale* **2015**, *7*, 3726.

(29) Panikkanvalappil, S. R.; Hira, S. M.; Mahmoud, M. A.; El-Sayed, M. A. *J. Am. Chem. Soc.* **2014**, *136*, 15961.

(30) Kang, B.; Austin, L. A.; El-Sayed, M. A. *ACS Nano* **2014**, *8*, 4883.

(31) Kang, J. W.; So, P. T. C.; Dasari, R. R.; Lim, D. K. *Nano Lett.* **2015**, *15*, 1766.

(32) Sisco, P. N.; Murphy, C. J. *J. Phys. Chem. A* **2009**, *113*, 3973.

(33) Olave, N.; Nicola, T.; Zhang, W.; Bulger, A.; James, M.; Oparil, S.; Chen, Y. F.; Ambalavanan, N. *Am. J. Physiol-Lung C* **2012**, *302*, L857.

(34) Claud, E. C.; Lu, J.; Wang, X. Q.; Abe, M.; Petrof, E. O.; Sun, J.; Nelson, D. J.; Marks, J.; Jilling, T. *Am. J. Physiol. Gastrointest. Liver Physiol.* **2008**, *294*, G1191.

(35) Meares, G. P.; Liu, Y. D.; Rajbhandari, R.; Qin, H. W.; Nozell, S. E.; Mobley, J. A.; Corbett, J. A.; Benveniste, E. N. *Mol. Cell. Biol.* **2014**, *34*, 3911.

(36) Hooshmand, N.; Bordley, J. A.; El-Sayed, M. A. *J. Phys. Chem. Lett.* **2014**, *5*, 2229.

(37) Schatz, G. C.; Van Duyne, R. P. In *Handbook of Vibrational Spectroscopy*; Chalmers, J. M., Griffiths, P. R., Eds.; Wiley: New York, 2002; Vol. *1*, pp 759−774.

(38) Kang, B.; Mackey, M. A.; El-Sayed, M. A. *J. Am. Chem. Soc.* **2010**, *132*, 1517.

(39) Vanwart, H. E.; Lewis, A.; Scheraga, H. A.; Saeva, F. D. *Proc. Natl. Acad. Sci. U. S. A.* **1973**, *70*, 2619.

DOI: 10.1021/jacs.5b13177
J. Am. Chem. Soc. 2016, 138, 3779−3788

(40) Maiti, N. C.; Apetri, M. M.; Zagorski, M. G.; Carey, P. R.; Anderson, V. E. *J. Am. Chem. Soc.* **2004**, *126*, 2399.
(41) Asher, S. A.; Ludwig, M.; Johnson, C. R. *J. Am. Chem. Soc.* **1986**, *108*, 3186.
(42) Hernandez, B.; Pfluger, F.; Kruglik, S. G.; Ghomi, M. *J. Raman Spectrosc.* **2013**, *44*, 827.
(43) Vaishnav, R. A.; Singh, I. N.; Miller, D. M.; Hall, E. D. *J. Neurotrauma* **2010**, *27*, 1311.
(44) Ray, P.; Devaux, Y.; Stolz, D. B.; Yarlagadda, M.; Watkins, S. C.; Lu, Y. B.; Chen, L.; Yang, X. F.; Ray, A. *Proc. Natl. Acad. Sci. U. S. A.* **2003**, *100*, 6098.
(45) Pogach, M. S.; Cao, Y. X.; Millien, G.; Ramirez, M. I.; Williams, M. C. *J. Cell. Biochem.* **2007**, *100*, 1415.
(46) Awasthi, S.; Gyurasics, A.; Knight, S. A.; Welty, S. E.; Smith, C. V. *Toxicol. Lett.* **1998**, *95*, 47.
(47) Sohal, R. S.; Agarwal, S.; Dubey, A.; Orr, W. C. *Proc. Natl. Acad. Sci. U. S. A.* **1993**, *90*, 7255.
(48) Spiro, T. G. *Biological Applications of Raman Spectroscopy*; Wiley: New York, 1987.
(49) Fodor, S. P. A.; Copeland, R. A.; Grygon, C. A.; Spiro, T. G. *J. Am. Chem. Soc.* **1989**, *111*, 5509.
(50) Beattie, J. R.; Bell, S. J.; Moss, B. *Lipids* **2004**, *39*, 407.
(51) Saxena, T.; Deng, B.; Stelzner, D.; Hasenwinkel, J.; Chaiken, J. *J. Biomed. Opt.* **2011**, *16*, 027003.
(52) Zhao, Y.; Ma, C.-Y.; Yuen, S.-N.; Phillips, D. L. *J. Agric. Food Chem.* **2004**, *52*, 1815.
(53) Takeda, M.; Iavazzo, R. E. S.; Garfinkel, D.; Scheinberg, I. H.; Edsall, J. T. *J. Am. Chem. Soc.* **1958**, *80*, 3813.
(54) Smith, H. A.; Reichardt, C. H. *J. Am. Chem. Soc.* **1941**, *63*, 605.
(55) Turner, N.; Grose, R. *Nat. Rev. Cancer* **2010**, *10*, 116.
(56) Yarden, Y. *Eur. J. Cancer* **2001**, *37*, S3.
(57) Normanno, N.; De Luca, A.; Bianco, C.; Strizzi, L.; Mancino, M.; Maiello, M. R.; Carotenuto, A.; De Feo, G.; Caponigro, F.; Salomon, D. S. *Gene* **2006**, *366*, 2.
(58) Hetz, C.; Chevet, E.; Oakes, S. A. *Nat. Cell Biol.* **2015**, *17*, 829.
(59) Schroder, M.; Kaufman, R. J. *Annu. Rev. Biochem.* **2005**, *74*, 739.
(60) Wang, S. Y.; Kaufman, R. J. *J. Cell Biol.* **2012**, *197*, 857.
(61) Hartl, F. U.; Hayer-Hartl, M. *Nat. Struct. Mol. Biol.* **2009**, *16*, 574.
(62) Soto, C. *Nat. Rev. Neurosci.* **2003**, *4*, 49.

DOI: 10.1021/jacs.5b13177
J. Am. Chem. Soc. 2016, 138, 3779−3788